DESY 08-053

ISSN 0418-9833
May 2008

Measurement of the Proton Structure Function $F_L(x, Q^2)$ at Low x

H1 Collaboration

Abstract

A first measurement is reported of the longitudinal proton structure function $F_L(x, Q^2)$ at the ep collider HERA. It is based on inclusive deep inelastic e^+p scattering cross section measurements with a positron beam energy of 27.5 GeV and proton beam energies of 920, 575 and 460 GeV. Employing the energy dependence of the cross section, F_L is measured in a range of squared four-momentum transfers $12 \leq Q^2 \leq 90$ GeV^2 and low Bjorken x $0.00024 \leq x \leq 0.0036$. The F_L values agree with higher order QCD calculations based on parton densities obtained using cross section data previously measured at HERA.

Submitted to Phys. Lett. **B**

F.D. Aaron[5,49], C. Alexa[5], V. Andreev[25], B. Antunovic[11], S. Aplin[11], A. Asmone[33], A. Astvatsatourov[4], A. Bacchetta[11], S. Backovic[30], A. Baghdasaryan[38], P. Baranov[25,†], E. Barrelet[29], W. Bartel[11], M. Beckingham[11], K. Begzsuren[35], O. Behnke[14], A. Belousov[25], N. Berger[40], J.C. Bizot[27], M.-O. Boenig[8], V. Boudry[28], I. Bozovic-Jelisavcic[2], J. Bracinik[3], G. Brandt[11], M. Brinkmann[11], V. Brisson[27], D. Bruncko[16], A. Bunyatyan[13,38], G. Buschhorn[26], L. Bystritskaya[24], A.J. Campbell[11], K.B. Cantun Avila[22], F. Cassol-Brunner[21], K. Cerny[32], V. Cerny[16,47], V. Chekelian[26], A. Cholewa[11], J.G. Contreras[22], J.A. Coughlan[6], G. Cozzika[10], J. Cvach[31], J.B. Dainton[18], K. Daum[37,43], M. Deák[11], Y. de Boer[11], B. Delcourt[27], M. Del Degan[40], J. Delvax[4], A. De Roeck[11,45], E.A. De Wolf[4], C. Diaconu[21], V. Dodonov[13], A. Dossanov[26], A. Dubak[30,46], G. Eckerlin[11], V. Efremenko[24], S. Egli[36], A. Eliseev[25], E. Elsen[11], S. Essenov[24], A. Falkiewicz[7], P.J.W. Faulkner[3], L. Favart[4], A. Fedotov[24], R. Felst[11], J. Feltesse[10,48], J. Ferencei[16], L. Finke[11], M. Fleischer[11], A. Fomenko[25], E. Gabathuler[18], J. Gayler[11], S. Ghazaryan[38], A. Glazov[11], I. Glushkov[39], L. Goerlich[7], M. Goettlich[12], N. Gogitidze[25], M. Gouzevitch[28], C. Grab[40], T. Greenshaw[18], B.R. Grell[11], G. Grindhammer[26], S. Habib[12,50], D. Haidt[11], M. Hansson[20], C. Helebrant[11], R.C.W. Henderson[17], H. Henschel[39], G. Herrera[23], M. Hildebrandt[36], K.H. Hiller[39], D. Hoffmann[21], R. Horisberger[36], A. Hovhannisyan[38], T. Hreus[4,44], M. Jacquet[27], M.E. Janssen[11], X. Janssen[4], V. Jemanov[12], L. Jönsson[20], D.P. Johnson[4,†], A.W. Jung[15], H. Jung[11], M. Kapichine[9], J. Katzy[11], I.R. Kenyon[3], C. Kiesling[26], M. Klein[18], C. Kleinwort[11], T. Klimkovich, T. Kluge[18], A. Knutsson[11], R. Kogler[26], V. Korbel[11], P. Kostka[39], M. Kraemer[11], K. Krastev[11], J. Kretzschmar[18], A. Kropivnitskaya[24], K. Krüger[15], K. Kutak[11], M.P.J. Landon[19], W. Lange[39], G. Laštovička-Medin[30], P. Laycock[18], A. Lebedev[25], G. Leibenguth[40], V. Lendermann[15], S. Levonian[11], G. Li[27], K. Lipka[12], A. Liptaj[26], B. List[12], J. List[11], N. Loktionova[25], R. Lopez-Fernandez[23], V. Lubimov[24], A.-I. Lucaci-Timoce[11], L. Lytkin[13], A. Makankine[9], E. Malinovski[25], P. Marage[4], Ll. Marti[11], H.-U. Martyn[1], S.J. Maxfield[18], A. Mehta[18], K. Meier[15], A.B. Meyer[11], H. Meyer[11], H. Meyer[37], J. Meyer[11], V. Michels[11], S. Mikocki[7], I. Milcewicz-Mika[7], F. Moreau[28], A. Morozov[9], J.V. Morris[6], M.U. Mozer[4], M. Mudrinic[2], K. Müller[41], P. Murín[16,44], K. Nankov[34], B. Naroska[12,†], Th. Naumann[39], P.R. Newman[3], C. Niebuhr[11], A. Nikiforov[11], G. Nowak[7], K. Nowak[41], M. Nozicka[11], B. Olivier[26], J.E. Olsson[11], S. Osman[20], D. Ozerov[24], V. Palichik[9], I. Panagoulias[l,11,42], M. Pandurovic[2], Th. Papadopoulou[l,11,42], C. Pascaud[27], G.D. Patel[18], O. Pejchal[32], H. Peng[11], E. Perez[10,45], A. Petrukhin[24], I. Picuric[30], S. Piec[39], D. Pitzl[11], R. Plačakytė[11], R. Polifka[32], B. Povh[13], T. Preda[5], V. Radescu[11], A.J. Rahmat[18], N. Raicevic[30], A. Raspiareza[26], T. Ravdandorj[35], P. Reimer[31], E. Rizvi[19], P. Robmann[41], B. Roland[4], R. Roosen[4], A. Rostovtsev[24], M. Rotaru[5], J.E. Ruiz Tabasco[22], Z. Rurikova[11], S. Rusakov[25], D. Salek[32], F. Salvaire[11], D.P.C. Sankey[6], M. Sauter[40], E. Sauvan[21], S. Schmidt[11], S. Schmitt[11], C. Schmitz[41], L. Schoeffel[10], A. Schöning[11,41], H.-C. Schultz-Coulon[15], F. Sefkow[11], R.N. Shaw-West[3], I. Sheviakov[25], L.N. Shtarkov[25], S. Shushkevich[26], T. Sloan[17], I. Smiljanic[2], P. Smirnov[25], Y. Soloviev[25], P. Sopicki[7], D. South[8], V. Spaskov[9], A. Specka[28], Z. Staykova[11], M. Steder[11], B. Stella[33], U. Straumann[41], D. Sunar[4], T. Sykora[4], V. Tchoulakov[9], G. Thompson[19], P.D. Thompson[3], T. Toll[11], F. Tomasz[16], T.H. Tran[27], D. Traynor[19], T.N. Trinh[21], P. Truöl[41], I. Tsakov[34], B. Tseepeldorj[35,51], I. Tsurin[39], J. Turnau[7], E. Tzamariudaki[26], K. Urban[15], A. Valkárová[32], C. Vallée[21], P. Van Mechelen[4], A. Vargas Trevino[11], Y. Vazdik[25], S. Vinokurova[11], V. Volchinski[38], D. Wegener[8], M. Wessels[11], Ch. Wissing[11], E. Wünsch[11], V. Yeganov[38], J. Žáček[32], J. Zálešák[31], Z. Zhang[27], A. Zhelezov[24], A. Zhokin[24], Y.C. Zhu[11], T. Zimmermann[40], H. Zohrabyan[38], and F. Zomer[27]

[1] I. Physikalisches Institut der RWTH, Aachen, Germany[a]
[2] Vinca Institute of Nuclear Sciences, Belgrade, Serbia
[3] School of Physics and Astronomy, University of Birmingham, Birmingham, UK[b]
[4] Inter-University Institute for High Energies ULB-VUB, Brussels; Universiteit Antwerpen, Antwerpen; Belgium[c]
[5] National Institute for Physics and Nuclear Engineering (NIPNE) , Bucharest, Romania
[6] Rutherford Appleton Laboratory, Chilton, Didcot, UK[b]
[7] Institute for Nuclear Physics, Cracow, Poland[d]
[8] Institut für Physik, TU Dortmund, Dortmund, Germany[a]
[9] Joint Institute for Nuclear Research, Dubna, Russia
[10] CEA, DSM/DAPNIA, CE-Saclay, Gif-sur-Yvette, France
[11] DESY, Hamburg, Germany
[12] Institut für Experimentalphysik, Universität Hamburg, Hamburg, Germany[a]
[13] Max-Planck-Institut für Kernphysik, Heidelberg, Germany
[14] Physikalisches Institut, Universität Heidelberg, Heidelberg, Germany[a]
[15] Kirchhoff-Institut für Physik, Universität Heidelberg, Heidelberg, Germany[a]
[16] Institute of Experimental Physics, Slovak Academy of Sciences, Košice, Slovak Republic[f]
[17] Department of Physics, University of Lancaster, Lancaster, UK[b]
[18] Department of Physics, University of Liverpool, Liverpool, UK[b]
[19] Queen Mary and Westfield College, London, UK[b]
[20] Physics Department, University of Lund, Lund, Sweden[g]
[21] CPPM, CNRS/IN2P3 - Univ. Mediterranee, Marseille - France
[22] Departamento de Fisica Aplicada, CINVESTAV, Mérida, Yucatán, México[j]
[23] Departamento de Fisica, CINVESTAV, México[j]
[24] Institute for Theoretical and Experimental Physics, Moscow, Russia
[25] Lebedev Physical Institute, Moscow, Russia[e]
[26] Max-Planck-Institut für Physik, München, Germany
[27] LAL, Univ Paris-Sud, CNRS/IN2P3, Orsay, France
[28] LLR, Ecole Polytechnique, IN2P3-CNRS, Palaiseau, France
[29] LPNHE, Universités Paris VI and VII, IN2P3-CNRS, Paris, France
[30] Faculty of Science, University of Montenegro, Podgorica, Montenegro[e]
[31] Institute of Physics, Academy of Sciences of the Czech Republic, Praha, Czech Republic[h]
[32] Faculty of Mathematics and Physics, Charles University, Praha, Czech Republic[h]
[33] Dipartimento di Fisica Università di Roma Tre and INFN Roma 3, Roma, Italy
[34] Institute for Nuclear Research and Nuclear Energy, Sofia, Bulgaria[e]
[35] Institute of Physics and Technology of the Mongolian Academy of Sciences , Ulaanbaatar, Mongolia
[36] Paul Scherrer Institut, Villigen, Switzerland
[37] Fachbereich C, Universität Wuppertal, Wuppertal, Germany
[38] Yerevan Physics Institute, Yerevan, Armenia
[39] DESY, Zeuthen, Germany
[40] Institut für Teilchenphysik, ETH, Zürich, Switzerland[i]
[41] Physik-Institut der Universität Zürich, Zürich, Switzerland[i]

[42] Also at Physics Department, National Technical University, Zografou Campus, GR-15773 Athens, Greece

[43] *Also at Rechenzentrum, Universität Wuppertal, Wuppertal, Germany*
[44] *Also at University of P.J. Šafárik, Košice, Slovak Republic*
[45] *Also at CERN, Geneva, Switzerland*
[46] *Also at Max-Planck-Institut für Physik, München, Germany*
[47] *Also at Comenius University, Bratislava, Slovak Republic*
[48] *Also at DESY and University Hamburg, Helmholtz Humboldt Research Award*
[49] *Also at Faculty of Physics, University of Bucharest, Bucharest, Romania*
[50] *Supported by a scholarship of the World Laboratory Björn Wiik Research Project*
[51] *Also at Ulaanbaatar University, Ulaanbaatar, Mongolia*

[†] *Deceased*

[a] *Supported by the Bundesministerium für Bildung und Forschung, FRG, under contract numbers 05 H1 1GUA /1, 05 H1 1PAA /1, 05 H1 1PAB /9, 05 H1 1PEA /6, 05 H1 1VHA /7 and 05 H1 1VHB /5*
[b] *Supported by the UK Science and Technology Facilities Council, and formerly by the UK Particle Physics and Astronomy Research Council*
[c] *Supported by FNRS-FWO-Vlaanderen, IISN-IIKW and IWT and by Interuniversity Attraction Poles Programme, Belgian Science Policy*
[d] *Partially Supported by Polish Ministry of Science and Higher Education, grant PBS/DESY/70/2006*
[e] *Supported by the Deutsche Forschungsgemeinschaft*
[f] *Supported by VEGA SR grant no. 2/7062/ 27*
[g] *Supported by the Swedish Natural Science Research Council*
[h] *Supported by the Ministry of Education of the Czech Republic under the projects LC527 and INGO-1P05LA259*
[i] *Supported by the Swiss National Science Foundation*
[j] *Supported by CONACYT, México, grant 48778-F*
[l] *This project is co-funded by the European Social Fund (75%) and National Resources (25%) - (EPEAEK II) - PYTHAGORAS II*

1 Introduction

This letter presents the first measurement of the longitudinal structure function $F_L(x, Q^2)$ of the proton at low Bjorken x. The inclusive deep inelastic ep scattering (DIS) cross section at low Q^2, written in reduced form as

$$\sigma_r(x, Q^2, y) = \frac{d^2\sigma}{dxdQ^2} \cdot \frac{Q^4 x}{2\pi\alpha^2 Y_+} = F_2(x, Q^2) - \frac{y^2}{Y_+} \cdot F_L(x, Q^2) \,, \tag{1}$$

is determined by two structure functions, F_2 and F_L. Here, $Q^2 = -q^2$ is the negative four-momentum squared transferred between the electron[1] and the proton, and $x = Q^2/2qP$ denotes the Bjorken variable, where P is the four-momentum of the proton. The two variables are related through the inelasticity of the scattering process, $y = Q^2/sx$, where $s = 4E_eE_p$ is the centre-of-mass energy squared determined from the electron and proton beam energies, E_e and E_p. In equation 1, α denotes the fine structure constant and $Y_+ = 1 + (1 - y)^2$.

The two proton structure functions F_L and F_2 are of complementary nature. They are related to the $\gamma^* p$ interaction cross sections of longitudinally and transversely polarised virtual photons, σ_L and σ_T, according to $F_L \propto \sigma_L$ and $F_2 \propto (\sigma_L + \sigma_T)$. Therefore the relation $0 \leq F_L \leq F_2$ holds. In the Quark Parton Model (QPM), F_2 is the sum of the quark and anti-quark x distributions, weighted by the square of the electric quark charges, whereas the value of F_L is zero [1]. In Quantum Chromodynamics (QCD), the longitudinal structure function differs from zero, receiving contributions from quarks and from gluons [2]. At low x and in the Q^2 region of deep inelastic scattering the gluon contribution greatly exceeds the quark contribution. Therefore F_L is a direct measure of the gluon distribution to a very good approximation. The gluon distribution is also constrained by the scaling violations of $F_2(x, Q^2)$ as described by the DGLAP QCD evolution equations [3]. An independent measurement of F_L at HERA, and its comparison with predictions derived from the gluon distribution extracted from the Q^2 evolution of $F_2(x, Q^2)$, thus represents a crucial test on the validity of perturbative QCD at low Bjorken x.

The longitudinal structure function, or the equivalent cross section ratio $R = \sigma_L/\sigma_T = F_L/(F_2 - F_L)$, was measured previously in fixed target experiments [4] and found to be small at large $x \geq 0.2$, confirming the QPM prediction in the Q^2 region of DIS.

From experimental determinations by H1 [5–7], which used assumptions on the behaviour of F_2 in extracting F_L, and from theoretical analyses of the inclusive DIS cross section data [8, 9], the longitudinal structure function at low x is expected to be significantly larger than zero. This prediction relies on perturbative QCD calculations of F_L to next-to-leading order (NLO) [10] and NNLO [11].

The measurement of F_L requires several sets of DIS cross sections at fixed x and Q^2 but at different y. This was achieved at HERA by variations of the proton beam energy whilst keeping the lepton beam energy fixed. The sensitivity to F_L is largest at high y as its contribution to σ_r is proportional to y^2. At low Q^2, high y values correspond to low values of the scattered electron energy. Small energy depositions can also be caused by hadronic final state particles leading to

[1]The term electron is used here to denote both electrons and positrons unless the charge state is specified explicitely. The data analysed are from positron-proton scattering, except for some measurements of background properties which additionally include electron-proton scattering data.

fake electron signals. These are dominantly due to photoproduction processes at $Q^2 \simeq 0$. The large size of this background makes the measurement of $F_L(x, Q^2)$ particularly challenging.

The present measurement of $F_L(x, Q^2)$ is based on data collected with the H1 detector in e^+p collisions from January to June 2007 with a positron beam energy of 27.5 GeV. Three proton beam energies were used, the largest, nominal energy of 920 GeV, the smallest energy of 460 GeV and an intermediate energy of 575 GeV, chosen for an approximately equal span between the three resulting cross section measurements in y^2/Y_+ (see equation 1). The integrated luminosities collected with H1 are $21.6\,\mathrm{pb}^{-1}$, $12.4\,\mathrm{pb}^{-1}$ and $6.2\,\mathrm{pb}^{-1}$, respectively. This letter presents first results on F_L in an intermediate range of Q^2, between 12 and 90 GeV^2.

2 Data Analysis

2.1 H1 Detector

The H1 detector [12] was built and upgraded for the accurate measurement of ep interactions at HERA. The detector components most relevant to this measurement are the central jet drift chamber (CJC), the central inner proportional chamber (CIP), the backward lead-scintillator calorimeter (SpaCal) and the liquid argon calorimeter (LAr). The CJC measures transverse momenta of tracks with an accuracy of $\delta p_t/p_t^2 \simeq 0.005$/GeV. Complementary tracking information is obtained from the backward silicon tracker (BST), which is positioned around the beam pipe, and from the z drift chamber COZ, which is located in between the two cylinders of the CJC. The CIP provides trigger information on central tracks [13]. The SpaCal [14] has an energy resolution of $\delta E/E \simeq 0.07/\sqrt{E/\mathrm{GeV}}$ for electromagnetic energy depositions and is complemented by a hadronic section. It also provides a trigger down to 2 GeV energy. The LAr allows the hadronic final state to be reconstructed with an energy resolution of about $0.50/\sqrt{E/\mathrm{GeV}}$.

Photoproduction events can be tagged with an electron calorimeter placed at $z = -6$ m downstream in the electron beam direction, which defines the negative z axis and thus the backward direction. The luminosity is determined from the Bethe-Heitler scattering process, which is measured using a photon calorimeter at $z = -103$ m.

2.2 Kinematic Reconstruction and Event Selection

The DIS kinematics at large y are most accurately reconstructed using the polar angle, θ_e, and the energy, E'_e, of the scattered electron according to

$$y = 1 - \frac{E'_e}{E_e}\sin^2(\theta_e/2)\ , \qquad Q^2 = \frac{{E'_e}^2\sin^2\theta_e}{1-y}\ , \tag{2}$$

where $x = Q^2/sy$. The event signature of this analysis comprises an electron scattered backwards and a well reconstructed event vertex. The scattered electron energy is measured in the backward calorimeter SpaCal. The polar angle is determined by the positions of the interaction vertex and the electron cluster in the SpaCal.

Energy E_e' of scattered electron candidate	> 3.4 GeV
Transverse size R_{log} of candidate cluster	< 5 cm
Hadronic energy fraction behind the cluster	$< 15\,\%$ of $E_e{}'$
Transverse distance between cluster and linked track	< 6 cm
$E - p_z$	> 35 GeV
z position of interaction vertex	$\lvert z_v \rvert < 35$ cm

Table 1: Criteria applied to select DIS events at high inelasticity y.

In order to trigger on low energy depositions with a threshold of 2 GeV, a dedicated trigger was developed based on the SpaCal cell energy depositions. At small energies the SpaCal trigger is complemented by the CIP track trigger which reduces the trigger rate to an acceptable level. The efficiency of this high y trigger is constant at around 98 % above 3 GeV, as monitored with independent triggers. At energies larger than 7 GeV no track condition is used in the trigger and the efficiency, up to highest energies, exceeds 99 %.

The event selection is based on the identification of the scattered electron as a localised energy deposition (cluster) of more than 3.4 GeV in the SpaCal. Hadrons, dominantly from photoproduction but also from DIS, may also lead to such energy depositions. This fake electron background is reduced by the requirement of a small transverse size of the cluster, R_{log}, which is estimated using a logarithmic energy weighted cluster radius. The background is further reduced by the requirement that the energy behind the cluster, measured in the hadronic part of the SpaCal, may not exceed a certain fraction of E_e'. For lower energies the selected cluster must be linked to a track. If the highest energy cluster fails to fulfill the selection criteria, the next to highest energy cluster passing the selection criteria is considered. Alternatively ordering the SpaCal clusters according to the scattering angle or transverse momentum gives consistent cross section results.

An additional suppression of photoproduction background is achieved by requiring longitudinal energy-momentum conservation using the variable

$$E - p_z = \Sigma_i (E_i - p_{z,i}) + E_e'(1 - \cos\theta_e), \qquad (3)$$

which for genuine, non-radiative DIS events is approximately equal to $2E_e$. Here E_i and $p_{z,i}$ are the energy and longitudinal momentum component of a particle i in the hadronic final state. This requirement also suppresses events with hard initial state photon radiation. QED Compton events are excluded using a topological cut against two back-to-back energy depositions in the SpaCal.

The selection is optimised to obtain large detection efficiency. This required detailed studies which were also based on high statistics event samples obtained in the years 2003-2006, corresponding to 51 pb^{-1} of e$^+$p and 45 pb^{-1} of e$^-$p interactions taken with a dedicated high y trigger at 920 GeV proton beam energy. The event selection criteria for the high y region are summarised in table 1.

The extraction of F_L also requires the measurement of cross sections at lower y. The low y region is defined for the 460 and 575 GeV data with $y < 0.38$ and for the 920 GeV data with $y < 0.5$. The analysis uses a method based on the electron variables for reconstruction and hence is limited to $y \geq 0.1$ for all data sets. The data at low y involve large polar angles θ_e outside the acceptance of the CJC. Therefore in this kinematic region no link to CJC tracks is required. At low y the photoproduction background is small and further reduced by a tightened cut on $R_{log} < 4\,\mathrm{cm}$.

2.3 Background Identification and Subtraction

At low E'_e, corresponding to high y, the remaining background contribution after the event selection may be of a size comparable to or even exceeding the genuine DIS signal. The method of background subtraction relies on the determination of the electric charge of the electron candidate from the curvature of the associated track.

Figure 1 shows the E/p distribution of the scattered electron candidates from e^+p interactions with the energy E measured in the SpaCal and the momentum p of the linked track determined by the CJC. The good momentum resolution leads to a clear distinction between the negative and positive charge distributions. The smaller peak corresponds to tracks with negative charge and thus represents almost pure background. These tracks are termed wrong sign tracks. The higher peak, due to right sign tracks, contains the genuine DIS signal superimposed on the remaining positive background. The size of the latter to first approximation equals the wrong sign background. The principal method of background subtraction, and thus of measuring the DIS cross section up to $y \simeq 0.9$, consists of the subtraction of the wrong sign from the right sign event distribution in each x, Q^2 interval.

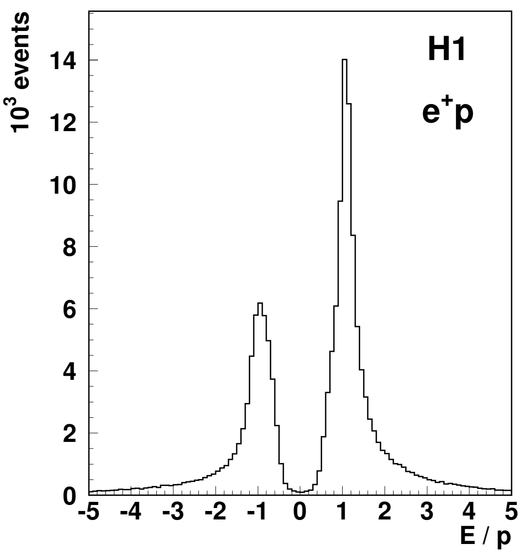

Figure 1: Distribution of energy over momentum for tracks linked to clusters in the SpaCal with energy from 3.4 to $10\,\mathrm{GeV}$ that pass all the cuts listed in table 1. Tracks with a negative charge are assigned a negative E/p.

The background subtraction based on the charge measurement requires a correction for a small but non-negligible charge asymmetry in the negative and positive background samples, as has been observed previously by H1 [6]. The main cause for this asymmetry lies in the enhanced energy deposited by anti-protons compared to protons at low energies. The most precise measurement of the background charge asymmetry has been obtained from comparisons of samples of negative tracks in e^+p scattering with samples of positive tracks in e^-p scattering. An asymmetry ratio of negative to positive tracks of 1.057 ± 0.006 is measured using the high statistics $e^{\pm}p$ data collected by H1 in 2003-2006. This result is verified using photoproduction events, with a tagged scattered electron, for which an asymmetry ratio of 1.06 ± 0.01 is measured. The difference in the hadronic final state between low and high proton beam energy data samples leads to an additional uncertainty of 0.003 on the asymmetry ratio.

The photoproduction background to the $E_p = 920\,\text{GeV}$ data, which are analysed at lower y than the low E_p data, is subtracted using a PHOJET [15] simulation normalised to the tagged photoproduction data. This background estimate agrees well with the corresponding result from the wrong sign analysis at high y.

2.4 Comparison of Data with Simulations

High statistics Monte Carlo (MC) simulations of DIS events are performed for the three proton beam energies using the DJANGO program [16], which includes leading order QED radiative corrections. The hadronic final state is simulated using ARIADNE [17], based on the Color Dipole Model, with subsequent fragmentation as described in JETSET [18]. The detector response is simulated using a program based on GEANT [19]. The simulated events are subject to the same reconstruction and analysis software as the data. The MC simulation uses a QCD parameterisation of the structure functions [7] normalised to the measured cross section.

Figure 2 shows, as an example, comparisons of the $460\,\text{GeV}$ high y data with simulated distributions, for the energy and the polar angle of the scattered electron prior to and after subtraction of the background which is determined using wrong sign data events. The DIS MC simulation corresponds to correct sign events with a small contribution from the wrong sign events subtracted. The latter are caused by events from lower Q^2 which can mimic an electron cluster at larger Q^2 and also by charge misidentification for the DIS events at the appropriate Q^2. The electron energy distribution after background correction is almost uniform. A similarly good agreement of the simulation with data has been observed for all other physics and technical variable distributions of relevance to this analysis, for all three data sets considered.

3 Cross Section Measurement

The scattering cross section is measured in the range $12 \leq Q^2 \leq 90\,\text{GeV}^2$ for Bjorken x of $0.00024 \leq x \leq 0.015$. The longitudinal structure function $F_L(x, Q^2)$ is extracted from three measurements of σ_r at fixed (x, Q^2) but different $y = Q^2/sx$. The data at lower E_p cover the higher y region. In the present analysis the cross section measurement is restricted to $0.1 \leq y \leq 0.56$ at $E_p = 920\,\text{GeV}$ and to $0.1 \leq y \leq 0.9$ at 460 and $575\,\text{GeV}$.

The measurement of F_L as described below relies on an accurate determination of the variation of the cross section for a given x and Q^2 at different beam energies. In order to reduce the

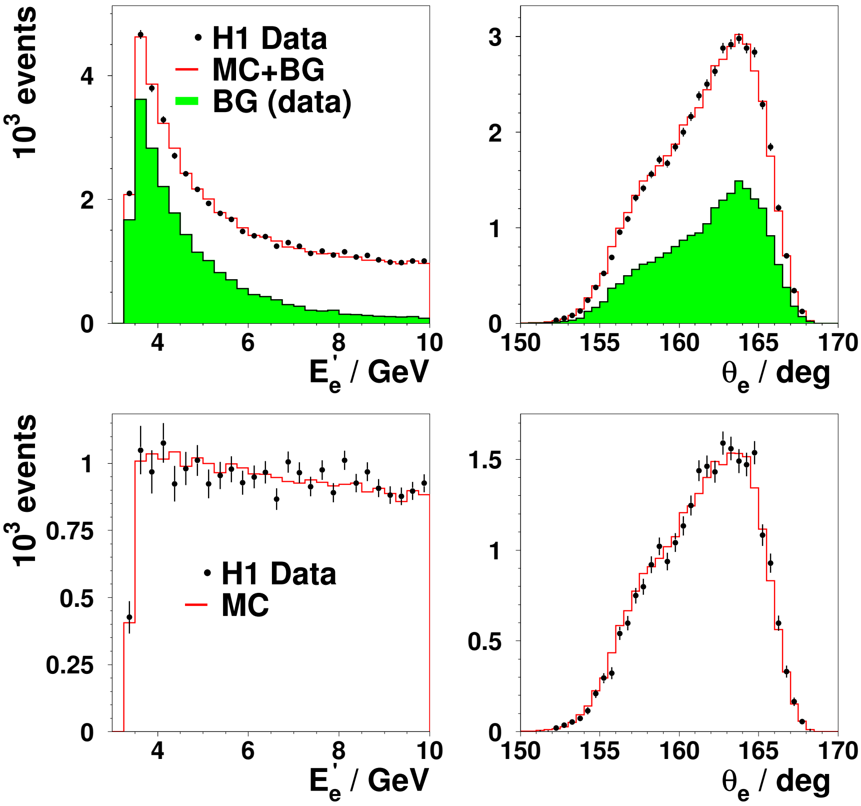

Figure 2: Top: comparison of the correct sign data (points) with the sum (open histogram) of the DIS MC simulation and background, determined from the wrong sign data (shadowed histogram), for the energy E'_e (left) and the polar angle θ_e (right) of the scattered electron, for the $460\,$GeV data with $E'_e < 10\,$GeV. Bottom: as top but after background subtraction.

uncertainty related to the luminosity measurement, which presently is known to 5% for each proton beam energy of the 2007 data used here, the three data samples are normalised relatively to each other. The renormalisation factors are determined at low y, where the cross section is determined by $F_2(x, Q^2)$ only, apart from a small correction due to R. Using weighted means of cross section ratios, extended over bins at low y, relative normalisation factors are derived to be 0.980, 0.995 and 1.010 for the 920, 575 and $460\,$GeV data, respectively. The relative normalisation is known to within 1.6%. This uncertainty comprises a systematic error of 1.4%, a statistical error of 0.6% and the residual influence of R is estimated to be 0.3%.

After background subtraction the data are corrected for detector efficiencies and for acceptances using the Monte Carlo simulations. The measured differential cross sections are consistent with the previous H1 measurement [6]. They are shown in figure 3. At large x values $\sigma_r \approx F_2$ and the three measurements are in good agreement. The cross sections rise towards low x but are observed to flatten and eventually turn over at very low x, corresponding to high values of y, where F_L is expected to contribute. This behaviour is consistent with the expectation as is illustrated using the cross section as implemented in the Monte Carlo simulation of the data.

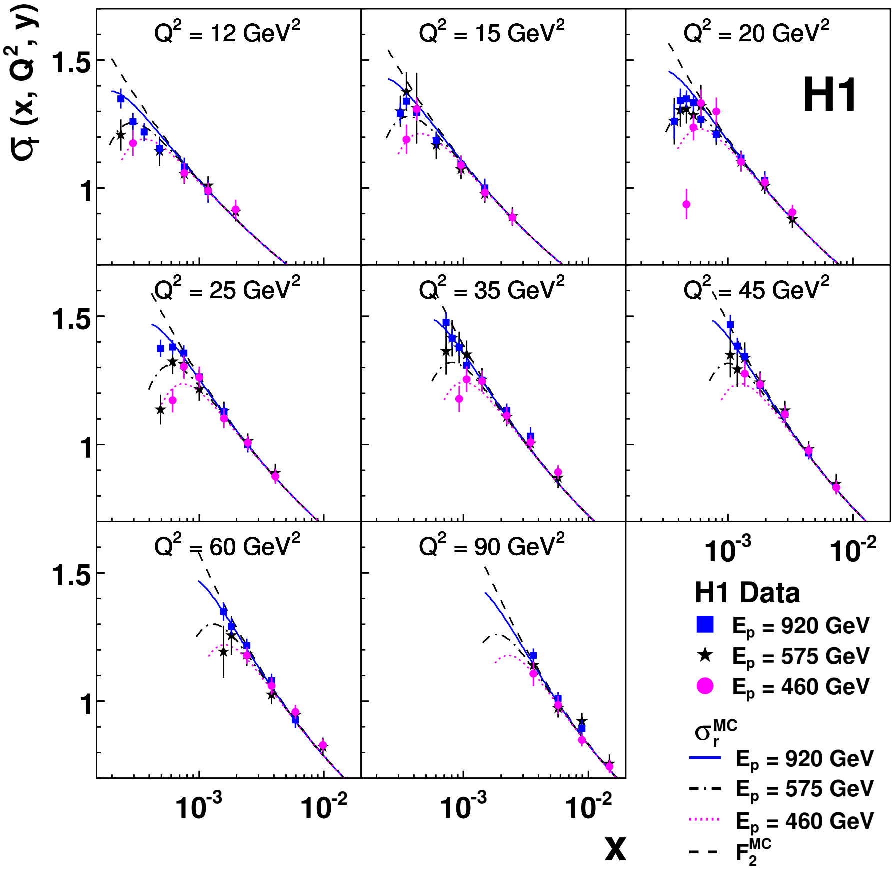

Figure 3: The reduced inclusive DIS cross sections measured at different Q^2 values and shown as a function of x for the data taken at the three proton beam energies, $920\,\mathrm{GeV}$ (squares), $575\,\mathrm{GeV}$ (stars) and $460\,\mathrm{GeV}$ (points). The error bars represent the statistical and systematic errors added in quadrature. The absolute luminosity uncertainty of the cross section measurement is not included in the error bars. Curves for σ_r as implemented in the Monte Carlo simulation of the data are shown as solid ($920\,\mathrm{GeV}$), dashed-dotted ($575\,\mathrm{GeV}$) and dotted lines ($460\,\mathrm{GeV}$) while the dashed line represents $F_2(x, Q^2)$, which is independent of s.

The systematic uncertainty on the cross section is derived from various contributions, some of which depend on the y region. The uncertainties leading to kinematic correlations are:

- The uncertainty on the SpaCal electromagnetic energy scale, determined with the double-angle method, is 0.4% at large energies degrading to 1% at $3\,\mathrm{GeV}$ energy. This is verified at the kinematic peak, where E_e' has to be close to E_e, and at lower energies with $\pi^0 \to \gamma\gamma$, $J/\Psi \to e^+e^-$ decays and with elastic QED Compton events.

- The uncertainty on the electron polar angle is 1 mrad, estimated using independent track information from the BST, the COZ and the CJC.

- The hadronic energy scale, calibrated using electron-hadron transverse and longitudinal momentum balance, has an uncertainty of 4%.
- The background charge asymmetry is known to 0.6% based on studies of wrong charge data in $e^{\pm}p$ scattering and tagged photoproduction events.
- The normalisation of the PHOJET simulation, used for background subtraction in the $920\,\text{GeV}$ data, has a 30% uncertainty.
- The central track-cluster link efficiency is verified with an independent track reconstruction using BST and CJC hit information. The uncertainty of this link efficiency combined with the interaction vertex reconstruction efficiency is estimated to be 1.5%. At low y, where no track link is required, the remaining uncertainty from the vertex reconstruction is 0.5%.

The uncorrelated systematic uncertainties originate from the Monte Carlo statistical errors and from the following sources:

- The uncertainty on the charge measurement is determined from data to Monte Carlo comparisons at low y and cross checked with radiative events which are background free in the low energy region. As the charge misidentification causes signal events to be subtracted as background, a 1% uncertainty on σ_r is obtained.
- The radiative corrections are efficiently reduced to below $10\,\%$ by the $E - p_z$ constraint and the topological cut against QED Compton events. A comparison of calculations based on the Monte Carlo simulation with the numerical program HECTOR [20] results in an uncertainty on σ_r of 1% at high y and 0.5% at low y.
- The trigger efficiency, determined from independent monitor triggers, is known to within 1% for the combined CIP–SpaCal trigger and 0.5% for the inclusive SpaCal trigger.
- Comparisons between different electron identification algorithms and between data and simulations yield an estimated uncertainty of 1% (0.5%) on the electron identification at high (low) y in the SpaCal calorimeter.

Further uncertainties, such as the effect of the LAr noise on the cross section, have been investigated and are found to be negligible. The subtraction of background using wrong sign tracks causes an additional statistical uncertainty which is included in the statistical error. The correlated and uncorrelated systematic errors combined with the statistical error lead to an uncertainty on the measured cross sections at high y of 3 to 5%, excluding the common luminosity error.

4 Measurement of $F_L(x, Q^2)$

The longitudinal structure function is extracted from the measurements of the reduced cross section as the slope of σ_r versus y^2/Y_+, as can be seen in equation 1. This procedure is illustrated in figure 4. At a given Q^2 value, the lowest x values are generally accessed by combining

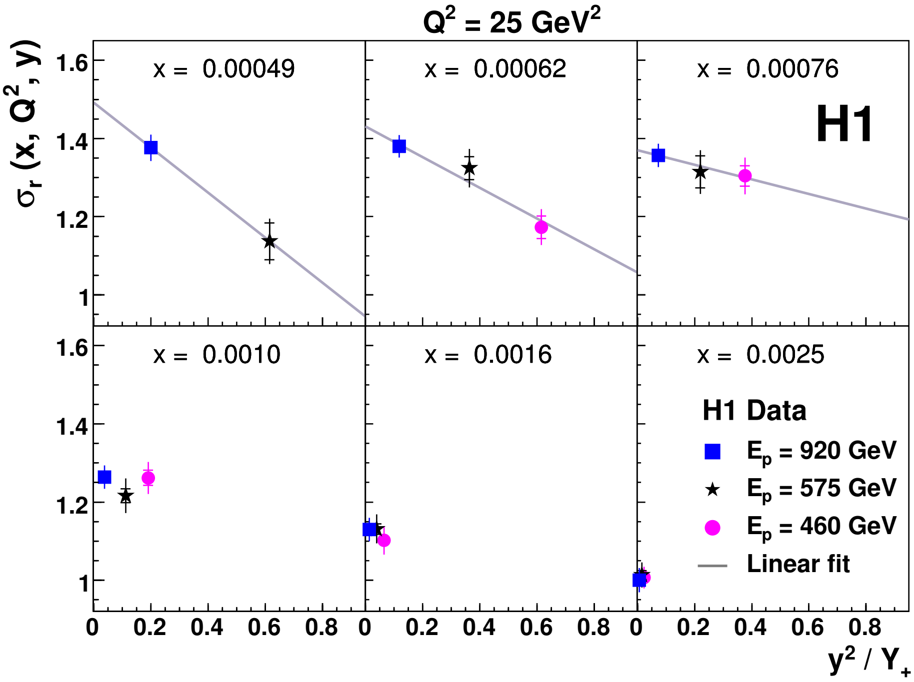

Figure 4: The reduced inclusive DIS cross section plotted as a function of y^2/Y_+ for six values of x at $Q^2 = 25\,\text{GeV}^2$, measured for proton beam energies of 920, 575 and 460 GeV. The inner error bars denote the statistical error, the full error bars include the systematic errors. The luminosity uncertainty is not included in the error bars. For the first three bins in x, corresponding to larger y, a straight line fit is shown, the slope of which determines $F_L(x, Q^2)$.

only the 920 and the 575 GeV data. At larger x, cross section measurements from all three data sets are available. These measurements are observed to be consistent with the expected linear dependence.

The central F_L values are determined in straight-line fits to $\sigma_r(x, Q^2, y)$ as a function of y^2/Y_+ using the statistical and uncorrelated systematic errors. The systematic errors on F_L take the correlations between the measurements into account using an off-set method: all correlated error sources, including the uncertainty from the relative normalisation of the cross sections which in the extraction of F_L is attributed to the 920 GeV cross sections, are considered separately and added in quadrature to obtain the total systematic error due to correlated sources. This error is added in quadrature to the statistical and uncorrelated systematic uncertainties to obtain the total error on F_L. The measurement is limited to bins where the total error is below 0.6.

The measurement of $F_L(x, Q^2)$ is shown in figure 5. The result is consistent with the prediction obtained with the H1 PDF 2000 fit [7], which was performed using only the H1 high energy cross section data. The measurement is also consistent with previous determinations of F_L by H1 [6], which used NLO QCD to describe and subtract the F_2 term from the measured reduced cross section at high y.

The values on $F_L(x, Q^2)$ resulting from averages over x at fixed Q^2 are presented in figure 6

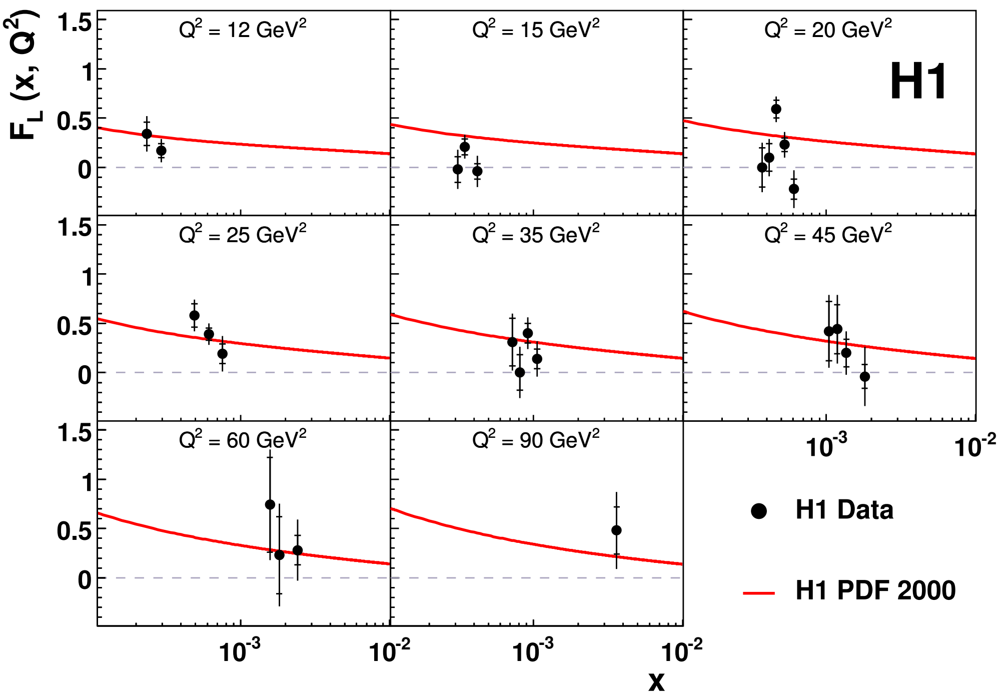

Figure 5: The longitudinal proton structure function $F_L(x, Q^2)$. The inner error bars denote the statistical error, the full error bars include the systematic errors. The luminosity uncertainty is not included in the error bars. The curve represents the NLO QCD prediction derived from the H1 PDF 2000 fit to previous H1 data.

and given in table 2. The average is performed taking the x dependent correlations between the systematic errors into account. The measurement of $F_L(x, Q^2)$ is compared with the H1 PDF 2000 fit and with the expectations from global parton distribution fits at higher order perturbation theory performed by the MSTW [8] and the CTEQ group [9] groups. Within the experimental uncertainties the data are consistent with these predictions. This consistency underlines the applicability of the DGLAP evolution framework of perturbative QCD at low Bjorken x at HERA.

5 Summary

This letter presents the first measurement of the longitudinal proton structure function in deep inelastic scattering at low x. The F_L values are extracted from three sets of cross section measurements at fixed x and Q^2, but different inelasticity y, obtained with three different proton beam energies at HERA. The results confirm DGLAP QCD predictions for $F_L(x, Q^2)$, determined from previous HERA data, which are dominated by a large gluon density at low x. At

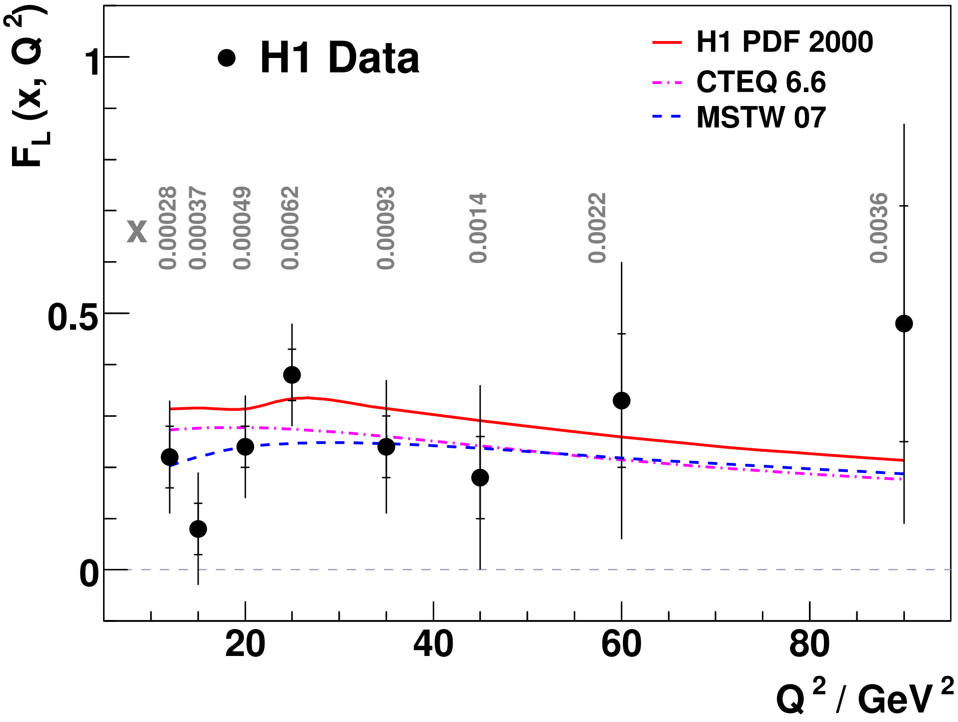

Figure 6: The longitudinal proton structure function F_L shown as a function of Q^2 at the given values of x. The inner error bars denote the statistical error, the full error bars include the systematic errors. The luminosity uncertainty is not included in the error bars. The solid curve describes the expectation on $F_L(x, Q^2)$ from the H1 PDF 2000 fit using NLO QCD. The dashed (dashed-dotted) curve is the expectation of the MSTW (CTEQ) group using NNLO (NLO) QCD. The theory curves connect predictions at the given (x, Q^2) values by linear extrapolation.

Q^2/GeV^2	x	F_L	stat.	uncorr.	corr.	total
12	0.00028	0.22	0.06	0.05	0.08	0.11
15	0.00037	0.08	0.05	0.04	0.09	0.11
20	0.00049	0.24	0.04	0.04	0.09	0.10
25	0.00062	0.38	0.05	0.05	0.08	0.10
35	0.00093	0.24	0.06	0.06	0.09	0.13
45	0.0014	0.18	0.08	0.08	0.14	0.18
60	0.0022	0.33	0.13	0.13	0.19	0.27
90	0.0036	0.48	0.23	0.22	0.22	0.39

Table 2: The longitudinal proton structure function $F_L(x, Q^2)$ measured at the given values of Q^2 and x. The statistical, uncorrelated and correlated systematic uncertainties are given as well as the total uncertainty.

the current level of accuracy, for the covered Q^2 range between 12 and $90\,\text{GeV}^2$, the data are thus consistent with perturbative QCD.

Acknowledgements

We are grateful to the HERA machine group whose outstanding efforts have made this experiment possible. We thank the engineers and technicians for their work in constructing and maintaining the H1 detector, our funding agencies for financial support, the DESY technical staff for continual assistance and the DESY directorate for support and for the hospitality which they extend to the non DESY members of the collaboration.

References

[1] C. Callan and D. Gross, Phys. Rev. Lett. **22** (1969) 156.

[2] A. Zee, F. Wilczek and S.B. Treiman, Phys. Rev. **D10** (1974) 2881;
G. Altarelli and G. Martinelli, Phys. Lett. **B76** (1978) 89.

[3] V.N. Gribov and L.N. Lipatov, Yad. Fiz. **15** (1972) 781 [Sov. J. Nucl. Phys. **15** (1972) 438];
V.N. Gribov and L.N. Lipatov, Yad. Fiz. **15** (1972) 1218 [Sov. J. Nucl. Phys. **15** (1972) 675];
Y.L. Dokshitzer, Sov. Phys. JETP **46** (1977) 641 [Zh. Eksp. Teor. Fiz. **73** (1977) 1216];
G. Altarelli and G. Parisi, Nucl. Phys. **B126** (1977) 298.

[4] J.J. Aubert *et al.*, EMC Collaboration, Phys. Lett. **B121** (1983) 87;
A.C. Benvenuti *et al.*, BCDMS Collaboration, Phys. Lett. **B223** (1989) 485;
L.W. Whitlow *et al.*, Phys. Lett. **B250** (1990) 193;
M. Arneodo *et al.*, NMC Collaboration, Nucl. Phys. **B483** (1997) 3 [hep-ex/9610231].

[5] C. Adloff *et al.*, H1 Collaboration, Phys. Lett. **B393** (1997) 452 [hep-ex/9611017].

[6] C. Adloff *et al.*, H1 Collaboration, Eur. Phys. J. **C21** (2001) 33 [hep-ex/0012053].

[7] C. Adloff *et al.*, H1 Collaboration, Eur. Phys. J. **C30** (2003) 1 [hep-ex/0304003].

[8] A.D. Martin, W.J. Stirling, R.S. Thorne and G. Watt, Phys. Lett. **B652** (2007) 292 [hep-ph/0706.0459].

[9] J. Pumplin, H.L. Lai and W.K. Tung, Phys. Rev. **D75** (2007) 054029 [hep-ph/0701220];
P.M. Nadolsky *et al.*, hep-ph/0802.0007.

[10] E.B. Zijlstra and W. van Neerven, Nucl. Phys. **B383** (1992) 525;
S.A. Larin and J.A.M. Vermaseren, Z.Phys. **C57** (1993) 93.

[11] S. Moch, J.A.M. Vermaseren and A. Vogt, Phys. Lett. **B606** (2005) 123, and references therein.

[12] I. Abt *et al.*, H1 Collaboration, Nucl. Instr. Meth. **A386** (1997) 310;
I. Abt *et al.*, H1 Collaboration, Nucl. Instr. Meth. **A386** (1997) 348.

[13] J. Becker *et al.*, Nucl. Inst. Meth. **A586** (2008) 190 [physics/0701002].

[14] R. Appuhn *et al.*, Nucl. Instr. and Meth. **A386** (1996) 397.

[15] R. Engel and J. Ranft, Phys. Rev. **D54** (1996) 4244 [hep-ph/9509373].

[16] G.A. Schuler and H. Spiesberger, Proc. Workshop on HERA Physics, Vol 3, eds. W. Buchmüller and G. Ingelman, Hamburg, DESY (1992), p. 1419;
A. Kwiatkowski, H. Spiesberger and H.-J. Möhring, Comp. Phys. Comm. **69** (1992) 155, version 1.14 of DJANGOH is used.

[17] L. Lönnblad, Comp. Phys. Comm. **71** (1992) 15, version 4.10 is used.

[18] T. Sjöstrand and M. Bengtsson, Comput. Phys. Comm. **43** (1987) 367, version 7.4 is used.

[19] R. Brun *et al.*, GEANT3, CERN Program Library, W5013.

[20] A. Arbuzov *et al.*, Comput. Phys. Comm. **94** (1996) 128 [hep-ph/9511434].